Axial Dispersion of Submicron Particles in Capillary Hydrodynamic Fractionation

In the present investigation, Taylor's analysis of the axial dispersion of a solute in a Newtonian fluid undergoing laminar flow through a circular tube was applied to dispersions of colloidal particles, in which effects of size exclusion, inertial and colloidal forces, and wall retardation must be considered. The results indicate that the product of the particle Reynolds and Peclet numbers determines the importance of the inertial forces on both the effective axial diffusion coefficient and the height of a theoretical plate.

The height of a theoretical plate as a function of the eluant ionic strength and average velocity, particle diameter, and tube diameter was determined experimentally. Close agreement with the numerical calculations from the diffusion equation was obtained. The height of a theoretical plate was found to attain a maximum value when the product of Reynolds and Peclet numbers was approximately 10.5.

Cesar A. Silebi
Jose G. DosRamos
Department of Chemical Engineering
and Emulsion Polymers Institute
Lehigh University
Bethlehem, PA 18015

Introduction

A slug of solute initially concentrated at the entrance of a capillary conduit spreads longitudinally as it moves with the carrier fluid. This spreading is referred to as axial dispersion. Knowledge of axial dispersion of species flowing through capillary conduits is important in many biological and physiological membrane transport processes. Some examples are the dispersion of soluble material in blood vessels and the dispersion of solutes in water-conducting organs of plants, as well as the fractionation of macromolecules in gel permeation chromatography (GPC) or of colloidal particles in hydrodynamic chromatography (HDC), capillary hydrodynamic fractionation (CHDF), and sedimentation field flow fractionation (SFFF). In gas chromatography, the principal advantage of using a narrow bore capillary, rather than packed chromatographic columns, lies in the considerably greater number of theoretical plates that can be generated in the narrow bore tubes due to the less amount of axial dispersion. In liquids, diffusion coefficients are about four orders of magnitude smaller than those in gases, which results in greater band broadening in a liquid mobile phase. Consequently, efforts have continually been made to apply the advantages of open tubes to high-performance liquid chromatography (HPLC).

The dispersion of molecular species in laminar flow through capillary tubes was first studied in 1953 by Taylor, who developed the theoretical analysis by which the longitudinal dispersion can be evaluated in terms of fundamental parameters. Shortly afterwards, Aris (1956) used the method of moments to generalize Taylor's analysis to include noncircular cross sections. The Taylor-Aris effective axial dispersion coefficient, D_{TA}, is given by:

$$D_{TA} = D_s + \frac{v_m^2 R_o^2}{48 D_s} \tag{1}$$

where
D_s = diffusion coefficient of the solute
R_o = radius of the capillary
v_m = average velocity of the fluid

Finite difference solutions have also been obtained by Bailey and Gogarty (1962) and Ananthakrishnan et al. (1965). The experimental data reported by Evans and Kennedy in 1965 confirm Taylor's theoretical prediction of average concentration distributions for large values of residence time. In 1970, DiMarzio and Guttman applied Taylor's analysis to evaluate longitudinal dispersion coefficients of finite-size spherical particles. According to DiMarzio and Guttman, a Brownian particle suspended in a viscous fluid undergoing Poiseuille flow within a capillary tube will sample all radial positions accessible to it with equal probability, provided the residence time in the flow field is long. Due to its finite size, however, the approach of the

Present address of J. G. DosRamos: Matec Applied Sciences, Hopkinton, MA.

particle center to the inner surface of the capillary tube will be limited to a distance equal to its radius. As a consequence of this, the particle is excluded from the slowest moving streamlines; this indicates that the longitudinal dispersion of particles will be somewhat decreased with increasing particle size. DiMarzio and Guttman obtained a modified Taylor-Aris axial dispersion coefficient, D^*_{DMG}, given by:

$$D^*_{DG} = D_\infty + \frac{v_m^2 R_o^2}{48 D_\infty}\left(1 - \frac{R_p}{R_o}\right)^6 \tag{2}$$

where R_p is the radius of the particles, D_∞ is the particle diffusivity in an unbounded fluid, given by the familiar Stokes-Einstein relation:

$$D_\infty = \frac{kT}{6\pi R_p \mu} \tag{3}$$

where

k = Boltzmann's constant
T = absolute temperature
μ = fluid viscosity

The term in parentheses in Eq. 2 accounts for the exclusion of the particle from a layer of thickness R_p around the wall.

Brenner and Gaydos (1977), following the method developed by Aris, also treated the problem of dispersion of particles in laminar flow within a capillary tube. This analysis used a more accurate representation of the particle velocity and its diffusion coefficient than that used by DiMarzio and Guttman, which is important since both the particle diffusion and diffusion coefficient are affected hydrodynamically by the presence of the capillary wall. Brenner and Gaydos' calculations indicate that the contribution of the convective flow to the axial dispersion as obtained by Taylor is decreased first by the DiMarzio exclusion effect up to an aspect ratio (the ratio of particle to capillary diameter) of 0.075, and then increased for larger aspect ratios due to the wall effect on the particle diffusion coefficient. Although Brenner and Gaydos did not include in their numerical calculations the effect of external and internal force fields, they did develop expressions from which the axial dispersion coefficient can be evaluated in the presence of such force fields.

Polymer colloids provide a model system with a broad range of well-characterized uniform particle sizes which can be used to further investigate the dispersion phenomena of particles flowing through capillary tubes under laminar flow conditions. Several experimental studies have been reported which demonstrate that, contrary to Taylor and Aris' analysis, when colloidal particles are pumped through a capillary tube, their axial dispersion decreased with increasing eluant velocities. Noel et al. (1978) were the first to report on such behavior for 10-μm particles when using capillary tubes to separate, according to size, of particles with diameters larger than 1 μm. In a similar study of particle fractionation by flow through capillaries, Brough et al. (1984) found the same behavior for 2-μm-diameter particles. These results and those of Poehlein (1979) have been reviewed by McHugh (1985) who explained them on the basis of the tubular pinch effect caused by the radial migration of the particles in laminar flow in tubes toward a noncentral radial position, due to the inertial forces (Segre and Silberberg, 1962). Ploehn (1987) analyzed the experimental results of Noel et al. (1978), for the mean axial velocity of the particle, by incorporating the inertial and colloidal forces into the general diffusive transport theory of Brenner and Gaydos (1977). Recently, Silebi and DosRamos (1988) used capillary hydrodynamic fractionation (CHDF) to obtain analytical separations of submicron-sized particles using capillaries with diameters as small as 7 μm. In contrast to previous studies, these investigators found that, when smaller capillaries are used in addition to the effect of the inertial forces on the particles, ionic strength effects were also of significant importance for the fractionation as well as for the axial dispersion.

In the present work, we follow Taylor's method of analysis of the dispersion phenomena in laminar flow through capillaries. The wall retardation effect, as well as the colloidal and inertial forces, are incorporated, since they affect the particle displacement and its radial distribution. The effect of these forces on the axial dispersion of colloidal particles, which have not been investigated previously, provides an interesting case for analysis, since the fluid flow is not complicated by the presence of the particle and the particle radial migration induced by the inertial and colloidal forces. The most important feature of the theory of dispersion as introduced by Taylor is that it enables one to describe the average concentration distribution in a complex three-dimensional system by the solution of the one-dimensional convective diffusion equation. As a result, the primary problem is to determine from first principles the dispersion coefficient associated with the one-dimensional diffusion equation.

The purpose of the present investigation is twofold: 1) to extend the analysis of dispersion of colloidal particles flowing through a circular tube by including the radial migration of the particles caused by inertial and colloidal forces; 2) to experimentally validate the analysis of dispersion obtained using various tube and particle diameters, fluid average velocities, and eluant ionic strengths.

Theory

Consider a capillary tube of length L and radius R_o through which a Newtonian fluid undergoes Poiseuille flow with an average velocity v_m. A dilute suspension of colloidal particles, of radius R_p, is injected at the entrance of the capillary, and the effluent is subsequently monitored. As the fluid carries the colloidal particles, the velocity profile and the various forces acting on the particles distort the slug and dispersion begins. Because of the finite size of the colloidal particles, their center of gravity is excluded from a layer of thickness R_p adjacent to the wall. As a consequence of this size effect, the center of gravity of the particles executes Brownian translation over a reduced cross-sectional area. This is illustrated in Figure 1.

A population balance of the colloidal particles in a small section of the capillary will include the flux of colloidal particles

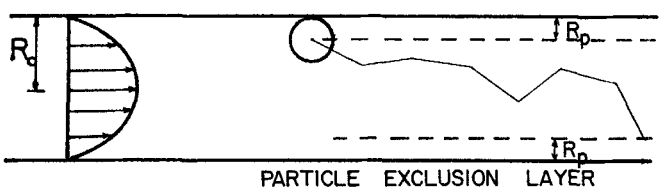

Figure 1. Streamline exclusion effect of a particle of radius R_p in a capillary tube of radius R_o.

due to the following phenomena:

- The convective flow of the colloidal particles being carried in the longitudinal direction by the flowing fluid
- Fickean diffusion of the particles due to radial and longitudinal gradients
- The forces of interaction between the capillary wall and the colloidal particles, mainly double layer repulsion and van der Waals attraction
- The fluid inertial forces acting on the particles

Thus, the total fluex, N, is given by the sum of the convective, Fickean, and colloidal-force-induced fluxes:

$$N = Cv_p - \boldsymbol{D} \cdot \nabla C - \frac{\boldsymbol{D}}{kT} \cdot \nabla \Phi \tag{4}$$

where Φ is the total potential of interaction between the particle and the surface of the capillary, given by the sum of the electrostatic double-layer repulsion and the van der Waals attractive potentials ($\Phi = \Phi_{DL} + \Phi_{VW}$), $\boldsymbol{D}$ and v_p are the diffusion coefficient tensor and the velocity of the particle.

Conservation and continuity of the concentration requires that C satisfy the continuity equation:

$$\frac{\partial C}{\partial t} + \nabla \cdot N = 0 \tag{5}$$

Substitution of the expressions for the fluxes into the equation of continuity gives:

$$\frac{\partial C}{\partial t} + \frac{1}{r}\frac{\partial}{\partial r}\left\{r\left[-D_r\frac{\partial C}{\partial r} + Cv_{p_r} + \frac{CD_r}{kT}\left(-\frac{\partial \Phi}{\partial r}\right)\right]\right\} + \frac{\partial}{\partial Z}\left(Cv_{p_z} - D_z\frac{\partial C}{\partial Z}\right) = 0 \tag{6}$$

where D_r and D_z are the radial and axial components of the particle diffusion coefficient tensor, both of which can be evaluated from the general Stokes-Einstein equation corrected for the proximity of the particle to the surface of the capillary:

$$\frac{D_i}{D_\infty} = 1 - \bar{\kappa}\bar{f}_i(\bar{r}) \tag{7}$$

where the dimensionless function, $\bar{f}_i$, is a correction to Stokes' law which is a function of the dimensionless radial position $\bar{r} = r/R_o$, available in tabular form (Hirschfield et al., 1984). In the direction parallel to the capillary wall, these tabulated values were evaluated in our calculations using the following expression:

$$\bar{f}_z(\bar{r}) = \frac{2.1044 - 2.75\bar{r} + 1.208\bar{r}^2}{1 - \bar{r}} \tag{8}$$

and in the direction perpendicular to the tube axis, the tabulated values of Hirschfield and Brenner were fitted by the following expression:

$$\bar{f}_r(\bar{r}) = \frac{1.8044 - 1.35\bar{r} + 0.671\bar{r}^2}{1 - \bar{r}} \tag{9}$$

Equation 6, together with the appropriate boundary and initial conditions, and the corresponding expressions for v_{p_z},v_{p_r} and the colloidal forces acting on the solute particle, describes the transport of colloidal particles through a capillary tube.

Fully-developed concentration profile

If the particle residence time in the capillary tube is long, the radial distribution of particle concentration downstream from the injection will attain steady state and the concentration profile will be fully developed. For this to occur, it is necessary that the particle residence time in the capillary, $\langle t_p \rangle$, be long enough for the particle to diffuse one capillary radius (which can be approximated by R_o^2/D_∞). For $\langle t_p \rangle$ greater than R_o^2/D_∞, the time required for convection to distort the slug is very long compared to the time for the concentration profile to relax vertically; therefore, the radial concentration profile can be expected to become fully developed. A comparison between the range of residence times for two different particle diameters (0.088 μm and 0.357 μm) with the diffusion time required for the particle to migrate one capillary radius by Brownian motion is shown in Table 1. In contrast to previous investigations (Noel et al., 1978; Poehlein, 1979; Brough et al., 1984), in the present work the particles have sufficient residence time to sample all possible radial positions several times, thus attaining steady state and a fully-developed concentration profile.

The solution for the fully-developed concentration profile can be obtained in a simpler manner than by solution of Eq. 6. At full development, the total flux, N_r, is zero. Thus,

$$N_r = -D_r\frac{\partial C}{\partial r} + Cv_{p_r} - \frac{CD_r}{kT}\frac{\partial \Phi}{\partial r} = 0 \tag{10}$$

Integration of this equation yields:

$$C(r) = C_m \frac{(R_o - R_p)^2 e^{-E(r)}}{2\int_0^{R_o - R_p} e^{-E(r)}\, r dr} \tag{11}$$

where

$$E(r) = \frac{\Phi}{kT} - \int_0^r \frac{v_{p_r}}{D_r(r)}\, dr \tag{12}$$

Table 1. The Smallest Experimental Elution Times vs. the Time Required for a Flowing Species to Travel across the Tube

		Particle Dia.	
Tube Radius, μm	Marker	88 nm	357 nm
3.75			
R_o^2/D_∞, s	0.01	2.8	11.5
Smallest Residence Time, s	210.0	190.0	165.0
6.5			
R_o^2/D_∞, s	0.03	8.5	34.6
Smallest Residence Time, s	210.0	200.0	190.0
17.0			
R_o^2/D_∞, s	0.2	58.0	237.0
Smallest Residence Time, s	900.0	850.0	800.0

and C_m, is the mean concentration in the tube which varies with axial position and time. If the particle's residence time in the capillary is much longer than R_o^2/D_∞, this equation can be assumed to hold for all Z.

Average particle velocity

At low particle concentrations, the probability density of a particle being at a particular radial position can be replaced by the number concentration, $C(r)$. Therefore, the average particle velocity can be calculated by weighting the local particle velocity at a given radial position with the concentration at that radial position (given by Eq. 11) and integrating over the cross section of the tube available to the particle. An expression results which is similar to those used to evaluate the average velocity of colloidal particles in hydrodynamic chromatography (Silebi and McHugh, 1978; Buffham, 1978; Prieve and Hoysan, 1978):

$$\langle v_{p_z} \rangle = \frac{\int_0^{R_o - R_p} v_{p_z}(r) e^{-E(r)}\, r dr}{\int_0^{R_o - R_p} e^{-E(r)}\, r dr} \tag{13}$$

The upper integration limit $(R_o - R_p)$ accounts for the finite size of the colloidal particle which excludes its center of gravity from a layer of thickness R_p adjacent to the wall as illustrated in Figure 1.

Local particle velocity

A particle suspended in a fluid undergoing Poiseuille flow is carried by the fluid at a velocity somewhat less than the axial velocity of the undisturbed fluid at the same distance from the tube wall as the particle's center of mass. The particle velocity at a distance r from the tube center is given by:

$$v_{p_z}(r) = 2v_m(1 - \bar{r}^2) - v_{p_s} \tag{14}$$

where the first term is the familiar laminar flow profile for the unperturbed eluant stream velocity which has a mean velocity v_m, at the position of the center of mass of the particle, and v_{p_s} is the slip velocity of the particle. In general, a neutrally buoyant particle lags the local Poiseuille flow in which it is suspended. For neutrally-buoyant particles, it has been found, both theoretically (Brenner and Happel, 1958) and experimentally (Goldsmith and Mason, 1961; Karnis et al., 1970), that the slip velocity of a particle suspended in a fluid flowing through a tube depends on the radial position of the particle and the ratio of particle radius to tube radius. Ho and Leal (1974) found that the simple addition of the two-single wall effects, used by Halow and Wils (1970) in a two-dimensional Poiseuille flow, gave results which compared well with their 'exact' results. Following Halow and Wils' approach, the resulting expression for v_{p_s} is:

$$v_{p_s} = \frac{4}{3} v_m \kappa^2 + \frac{5}{4} v_m \kappa^3 (1 + \bar{r}) \cdot \left[\frac{1}{(1 - \bar{r})^2} - \frac{1}{(1 + \bar{r})^2}\right] + O(\kappa^3) \tag{15}$$

This expression is consistent with the experimental results of Goldsmith and Mason (1961), as well as with the theoretical analysis of the slip velocity of a particle in a capillary tube by Bungay and Brenner (1979).

Radial velocity

The hydrodynamic lateral force, which drives the particles toward a certain equilibrium radial position at about 60% of the tube radius from the tube axis, as observed by Segre and Silberberg (1962a, b), has been the subject of numerous theoretical analyses (Rubinow and Keller, 1961; Safman, 1965). Most of these investigators obtained expressions which did not predict this asymmetric equilibrium radial position, and an empirical factor was introduced in their equations to account for this experimental observation. Cox and Brenner (1968) developed the theory from which the particle's radial migration velocity, v_{p_r}, in a general tube flow can be calculated. The radial migration velocity of a freely-rotating particle in a general bounded flow is given by (Cox and Brenner, 1968):

$$v_{p_r} = \frac{6\pi R_p}{\nu}\left\{U_\infty^2 h\left(\frac{r}{R_o}\right) - U_\infty v_m g\left(\frac{r}{R_o}\right) + \frac{5}{9} v_m^2 \kappa^2 \left[f_1\left(\frac{r}{R_o}\right) + f_2\left(\frac{r}{R_o}\right)\right]\right\} \tag{16}$$

where ν is the kinematic viscosity of the fluid, and U_∞ is the sedimentation velocity of the particle in an unbounded fluid. In this analysis, in which the wall effects were not considered, the axial slip velocity due to buoyancy effects is simply U_∞. Using this general theory, Ho and Leal (1974) and Cox and Hsu (1977) determined the radial velocity of a particle in simple shear flow and in one- and two-dimensional Poiseuille flows, respectively. These theoretical analyses showed that when a particle lags the flowing fluid, it will migrate away from both the axis of symmetry and the plane surface bounding the fluid. Recently, Ishii and Hasimoto (1980) succeeded in determining the migration velocity of a particle in a circular tube using the general theory of Cox and Brenner (1968) and the expressions of the Green's function obtained earlier by Hasimoto (1977). Since the theoretical calculations of Ishii and Hasimoto break down near the wall of the capillary, we, like Ishii and Hasimoto, used the theoretical values obtained by Cox and Hsu in this region. In order to simplify our calculations, the theoretical curves for the functions h, g, f_1, and f_2 shown in Figures 1, 2 and 3a of Ishii and Hasimoto (1980), which include the asymptotic values obtained by Cox and Hsu near the capillary surface, were fitted by the following expressions:

$$h\left(\frac{r}{R_o}\right) = -\frac{0.207}{6\pi}\left[\frac{r}{R_o} - 0.53\left(\frac{r}{R_o}\right)^2\right] \tag{17}$$

$$g\left(\frac{r}{R_o}\right) = -\frac{0.144}{6\pi}\left[\frac{r}{R_o} - \left(\frac{r}{R_o}\right)^6\right] \tag{18}$$

$$f_1\left(\frac{r}{R_o}\right) + f_2\left(\frac{r}{R_o}\right) = \frac{0.721}{\pi}\left(\frac{r}{R_o}\right)\left(0.71 - \frac{r}{R_o}\right)\exp\left(\frac{0.786r}{R_o}\right) \tag{19}$$

Substituting these expressions into Eq. 16 permits determination of the radial migration velocity of a particle in a tube. In the case of neutrally-buoyant particles, the sedimentation velocity is zero and, therefore, the first two terms in Eq. 16 are zero; inde-

pendent of the ratio of particle to tube ratio, this equation predicts an equilibrium radial position, in which v_{p_r} is zero, at $r/R_o = 0.71$. Karnis et al. (1966) and Walz and Grun (1973), however, found that the equilibrium radial position for neutrally buoyant particles varies with the ratio of particle to tube radius when the tube Reynolds number is less than 1. In the absence of a rigorous solution to account for these effects, we used the following approach: rather than using the axial slip velocity in the absence of wall effects, U_∞, in Eq. 16, we used the axial slip velocity when wall effects are not negligible, as given by (Brenner, 1966):

$$U = U_\infty[1 - \kappa \bar{f}_3(\bar{r})] - v_{p_r} \tag{20}$$

where $\bar{f}_3(\bar{r})$ is the correction for the terminal setting velocity of the particle in a bounded fluid (Brenner, 1966). As indicated in Table 2, our calculated values of the equilibrium radial position, using the approach described above, at those values of κ are essentially identical to the values reported by Karnis et al. (1966) and also to those obtained using the correlation derived by Walz and Grun (1973) which is based on curve fitting the experimentally-determined radial equilibrium positions obtained at Reynolds numbers less than 1.

Colloidal forces

The potentials of interaction, Φ_{DL} and Φ_{vw}, are calculated by assuming a sphere-plane interaction, a justifiable assumption because of the small ratio of particle to capillary radii. Approximate expressions for the double-layer repulsion covering the range from small- to large-particle-wall separations have been developed by Bell (1970) and Oshima et al. (1982). The appropriate formulas are:

$$\Phi_{DL} = \frac{32\epsilon\left(\frac{kT}{e}\right)^2 \tanh\left(\frac{e\Psi_1}{4kT}\right)\tanh\left(\frac{e\Psi_2}{2kT}\right)R_p \exp\left(-\frac{a}{\kappa_D}\right)}{1 + \left[1 - \frac{2R_p/\kappa_D + 1}{(R_p/\kappa_D + 1)^2}\tanh^2\left(\frac{e\Psi_2}{4kT}\right)\right]^{1/2}} \tag{21}$$

where

ϵ = dielectric constant of the eluant
e = protonic charge
a = minimum separation distance between the particle and capillary surfaces, $R_o - r - R_p$
Ψ_i = surface potentials for the capillary, $i = 1$, or particle, $i = 2$
κ_D = Debye double-layer thickness, in terms of the ionic concentration in the eluant phase, c_i, and for a symmetric electrolyte of valence z

Table 2. Values of the Equilibrium Radial Position, r^*, as a Function of the Ratio of Particle to Capillary Radius, κ

κ	r^* from Eq. 27 Substit. U_∞ by U	Walz and Grun (1973) $r^* = 0.67\,(1 - \kappa)$
0.01	0.659	0.663
0.04	0.636	0.643
0.07	0.617	0.623
0.10	0.599	0.603
0.13	0.583	0.583
0.16	0.568	0.563

Thus,

$$\kappa_D = \sqrt{\frac{\epsilon kT}{8\pi e^2 z c_i}} \tag{22}$$

The latex surface potential, Ψ_2, which is a function of surface charge density, σ_q, and the molar concentration of ionic species, c_i, and for symmetric electrolytes is given by (Hamaker, 1937):

$$\sigma_q = \sqrt{\frac{2\epsilon kTc_i}{\pi}}\sinh\left(\frac{ze\Psi_2}{2kT}\right) \tag{23}$$

The total surface charge density in the presence of the surfactant can be evaluated by conductometric titration or indirectly from measurement of the zeta potential at a particular ionic strength.

The van der Waals attractive potential between a sphere and a plane wall was originally estimated by Hamaker (1937) based on the unretarded attraction energy between two atoms. More recently, Gregory (1981) derived an approximate expression accounting for the retardation effects which must be considered at large separations:

$$\Phi_{vw} = -\frac{A_H R_p}{6a}\frac{1}{1 + \frac{14a}{\lambda}} \tag{24}$$

where A_H is Hamaker's constant and λ is the wavelength of intrinsic oscillations of atoms which can be derived from refractive index data (Ottewill and Healy, 1962).

Since Born repulsive forces are very short-range interactions, they are of negligible importance. Because low-molecular-weight anionic surfactants have been used in our experiments, steric repulsion potentials have not been included in our calculations.

Effective mean axial diffusion coefficient

Following Taylor's analysis, it is convenient to define concentration and velocity relative to axes moving with the average velocity of the colloidal particles. The axial distance Z_1 measured from the origin of this coordinate system is given by:

$$Z_1 = Z - \langle v_{p_z}\rangle t \tag{25}$$

where Z is the position relative to the tube entrance. In this moving coordinate system, the time derivative may be neglected since the concentration profile evolves very slowly in the translating coordinate system. After neglecting the contribution to the flux of the colloidal particles by axial diffusion (Taylor, 1954), in this moving coordinate system Eq. 6 in dimensionless form reduces to:

$$\frac{1}{\bar{r}}\frac{\partial}{\partial\bar{r}}\left\{\bar{r}\left[-\bar{D}_r\frac{\partial\bar{C}}{\partial\bar{r}} + \bar{C}\left(\frac{3}{8}Re_pP_e\bar{v}_{p_r} - \bar{D}_r\frac{\partial\bar{\Phi}}{\partial\bar{r}}\right)\right]\right\} + (\bar{v}_{p_z} - R_f)\frac{\partial\bar{C}}{\partial\bar{Z}_1} = 0 \tag{26}$$

where the following set of dimensionless variables have been introduced:

$$\bar{r} = r/R_o \quad \bar{v}_{p_z} = v_{p_z}/v_m \quad \bar{Z}_1 = Z_1 D_\infty / v_m R_o^2 \quad \bar{\Phi} = \Phi/kT$$

$$\bar{v}_{p_r} = \frac{v_{p_r} \nu}{v_m^2 R_p^2 \kappa^2} \quad \bar{C} = C/C_o \quad \bar{D}_r(r) = D_r(r)/D_\infty \tag{27}$$

where the particle Reynolds number, Re_p, the Peclet number, Pe, and the separation factor, R_f are given by:

$$Re_p = \frac{2R_p\left(\frac{4}{3}\right) v_m \kappa^2}{\nu} \quad Pe = \frac{R_o v_m}{D_\infty} \quad R_f = \frac{\langle v_{p_z} \rangle}{v_m} \tag{28}$$

Integrating twice with respect to $\bar{r}$ yields:

$$\bar{C} = \bar{C}_m + \frac{\partial \bar{C}_m}{\partial \bar{Z}_1} \int_0^{\bar{r}} \frac{H(\bar{r}^*)\, d\bar{r}^*}{\bar{r}^* \bar{D}(\bar{r}^*) e^{-E(\bar{r}^*)}} \tag{29}$$

where

$$H(\bar{r}^*) = \int_0^{\bar{r}^*} \{\bar{v}_{p_z}(\bar{r}^{**}) - R_f\} e^{-E(\bar{r}^{**})} \bar{r}^{**}\, d\bar{r}^{**} \tag{30}$$

Defining $N_{Z_1}(Z_1, t)$ as the rate of transport of particles across a plane of constant Z_1, the following expression is obtained:

$$N_{Z_1} = 2\pi \int_0^{R_o - R_p} \left\{ C(v_{p_z} - \langle v_{p_z} \rangle) - D_z \frac{\partial C}{\partial Z_1} \right\} r\, dr \tag{31}$$

Substituting Eqs. 11 and 29 into Eq. 31 produces:

$$N_{Z_1} = 2\pi \frac{\partial C_m}{\partial Z_1} \int_0^{R_o - R_p} \cdot \left\{ [v_{p_z} - \langle v_{p_z} \rangle] \int_0^r \frac{H(r^*)\, dr^*}{D_r(r^*) e^{-E(r^*)}} - D_z(r) \right\} e^{-E(r)}\, r dr \tag{32}$$

Integrating by parts the double integral in Eq. 31, and substituting Eqs. 13 and 29 we obtain:

$$N_{Z_1} = -2\pi \frac{\partial C_m}{\partial Z_1} \left\{ \int_0^{R_o - R_p} \frac{H^2(r)}{r D_r(r) E^{-E(r)}}\, dr + \int_0^{R_o - R_p} D_z(r) e^{-E(r)}\, r dr \right\} \tag{33}$$

The time rate of change in the number of particles in a thin slice, bounded by the planes Z_1 and $Z_1 + dZ_1$, is equal to the net flow of particles through the two planes:

$$2\pi \frac{\partial}{\partial t} \left(\int_0^{R_o - R_p} C r\, dr \right) = -\frac{\partial N_{Z_1}}{\partial Z_1} \tag{34}$$

By substituting Eqs. 11 and 32 into Eq. 33, the following expression is obtained:

$$\frac{\partial \bar{C}_m}{\partial t} = D^* \frac{\partial^2 \bar{C}_m}{\partial Z_1^2} \tag{35}$$

where

$$D^* = \frac{\int_0^{R_o - R_p} \frac{H^2(r)\, dr}{r D_r(r) e^{-E(r)}}}{\int_0^{R_o - R_p} e^{-E(r)} r\, dr} + \frac{\int_0^{R_o - R_p} D_z(r) e^{-E(r)} r\, dr}{\int_0^{R_o - R_p} e^{-E(r)} r\, dr} \tag{36}$$

which is the effective axial dispersion coefficient for the convective transport of colloidal species through a tube. This is the same result obtained by Brenner and Gaydos using Aris' formalism.

The solution to Eq. 35 in the case in which N particles are concentrated over a small length δL at the capillary entrance ($z = 0$), at time $t = 0$, is given by:

$$C_m = \frac{N}{2R_o^2 \sqrt{\pi^3 D^* t}} e^{-(Z_1^2/4D^* t)} \tag{37}$$

The equations for the particle velocity and the colloidal and inertial forces were combined with Eqs. 7, 12 and 30 to compute from Eq. 36 the effective axial diffusion coefficient of colloidal particles flowing through a narrow bore capillary as a function of experimentally-measured parameters—eluant ionic strength and average velocity, capillary inner diameter, and colloid particle diameter, as well as the material parameters—Hamaker constant, surface charge density, and/or surface potential.

Results and Discussion

Effect of size exclusion and wall resistance

In order to consider the size exclusion and wall effects, we have set the potential $E(r)$ equal to zero. As a consequence, the exponential terms in Eqs. 13, 30 and 36 are equal to 1, which indicates that a particle samples all possible radial positions with equal probability. The dimensionless effective diffusion coefficient given by the ratio of the effective diffusion coefficient of the particles (obtained from the numerical integration of Eq. 36) to the effective diffusion coefficient given by the Taylor-Aris theory (Eq. 1) is shown in Figure 2 for three cases.

The first case (curve A) corresponds to the results of DiMarzio and Guttman's analysis, which considers the effects of: i) the exclusion of the particle center from the region close to the tube wall; and ii) the velocity retardation effect of the particle given by the leading term of the slip velocity expression in Eq. 15. Because of the exclusion effect, particles do not sample the smaller fluid velocities. As a consequence, the axial spreading of particles is decreased as the size of the exclusion layer is increased (larger particle sizes). On the other hand, the velocity retardation of the particles should increase their axial spreading. Because the exclusion effect is first-order (first power dependence on the ratio of particle to capillary radii), while the velocity retardation is second order, the net result of these two effects is a decrease in the effective axial dispersion coefficient, as shown in Figure 2. The results of our numerical calculations are essentially identical to the analytical expression derived by DiMarzio and Guttman (Eq. 2).

The second case (curve B) corresponds to the zero potential results obtained by Brenner and Gaydos, which include not only the two effects considered by DiMarzio and Guttman, but also the complete expression for the slip velocity, as well as the hydrodynamic wall effects in the translational diffusivity. This

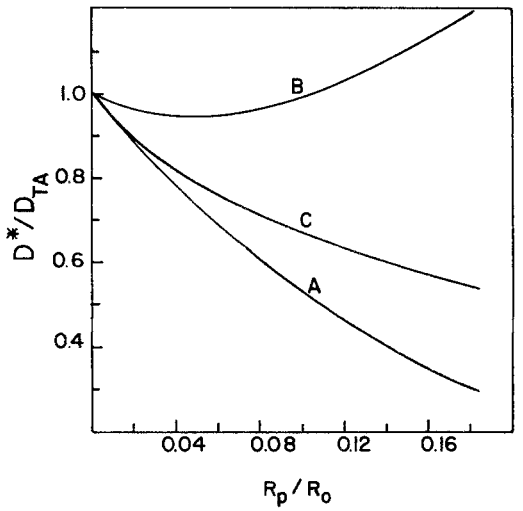

Figure 2. Dimensionless axial diffusion coefficient of colloidal particles at zero potential.

Curve A, DiMarzio and Guttman's case (slip velocity given by first term in Eq. 15); B, Brenner and Gaydos' case; C, DiMarzio and Guttman's case (slip velocity given by Eq. 15).

diffusivity goes to zero when the sphere is in contact with the wall due to the finite hydrodynamic resistance to translational motion (both parallel and perpendicular to the wall) of a sphere in contact with the wall. Since the translational diffusivity of the particles decreases as the hydrodynamic resistance to translational motion increases, this effect increases the first term in Eq. 36 while the second term decreases. The second term, however, is several orders of magnitude smaller than the first term in Eq. 36; consequently, the effective axial dispersion coefficient is increased by the enhancement of the hydrodynamic resistance to translational motion of the particles near the wall. The results of our calculations for this case are shown in curve B of Figure 2. It can be seen that the relative effective diffusion coefficient decreases for particles whose ratio of particle to capillary radius is smaller than 0.075, attaining a minimum at about this ratio of particle to capillary radius. This indicates that, for the smaller particle sizes, the exclusion effect is dominant. On the other hand, for ratios of particle to capillary radii greater than 0.075, the relative diffusion coefficient increases as the particle size increases due to the effect of the increase in hydrodynamic resistance to translational diffusivity which then becomes the controlling mechanism. Our numerical calculations, obtained using the equations described in this paper (curve B), agree quite well with the results of Brenner and Gaydos.

In the third case (curve C), we carried a sensitivity study of the effect of the slip velocity by considering in the first case (DiMarzio and Guttman) the complete expression of the slip velocity given by Eq. 26. As discussed above, an increase in the slip velocity, specially in the region near the wall, will result in an increase in the effective diffusion coefficient as mentioned before. The increase of the effective diffusion coefficient over the values obtained in the first case (curve A) was not substantial enough to produce an upturn in the relative effective longitudinal diffusion coefficient as the particle size increases over the same range of particle to capillary radii. In another set of calculations, we set the slip velocity equal to zero everywhere in the capillary and obtained identical results as in the first case. These results point out the importance of the hydrodynamic effects in the regions near the capillary wall for the determination of the actual effective axial diffusion coefficient of the particles.

Effect of the inertial force of the fluid on the particle

The effect on the radial distribution of particles by the radial force exerted by the fluid on a neutrally buoyant particle suspended in a Poiseuille flow field is determined by the particle radial velocity (which depends upon the slip velocity of the particle), the radial component of the diffusivity tensor, the radius of the particle, and the radius of the capillary tube. As can be seen in the coefficient of the radial velocity term in Eq. 26 (which will also become the coefficient of the integral expression in the exponential term of Eq. 11), these parameters can be lumped into the product of the particle Reynolds number, Re_p, the Peclet number, Pe and the dimensionless integral which accounts for the radial dependence of the radial velocity and the radial component of the diffusivity tensor. We have found that this integral has only a weak dependence on the ratio of particle radius to the capillary radius. Thus, the effect of the inertial force will be determined primarily by the magnitude of the product Re_pPe which depend upon the following variables: the eluant average velocity, particle size, and tube inner diameter. In this section, we will discuss the effect of each one of these variables. Two sets of calculations were performed. In the first case, the colloidal forces were neglected. In the second case, the colloidal forces were included in the calculations with an electrolyte concentration of 1 mM. The effect of varying the electrolyte concentration will be discussed in the next section.

The effect of the eluant average velocity on the effective diffusion coefficient of the colloidal particles is shown in Figures 3 and 4 for two capillary radii and particles smaller than 1 μm. In these calculations we set the colloidal forces equal to zero. For particles whose radius is smaller than 0.1 μm, the effective diffusion coefficient is not significantly affected by variations in the eluant average velocity. This can be attributed to the fact that

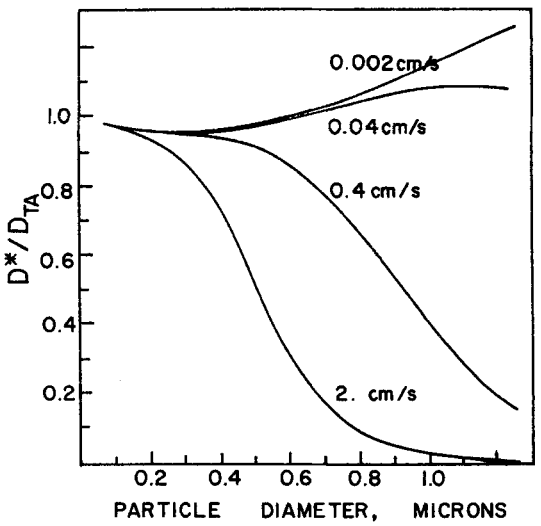

Figure 3. Theoretical results for the dimensionless axial diffusion coefficient of colloidal particles vs. particle size at different eluant average velocities.

Colloidal forces are not included; capillary diameter, 6 μm.

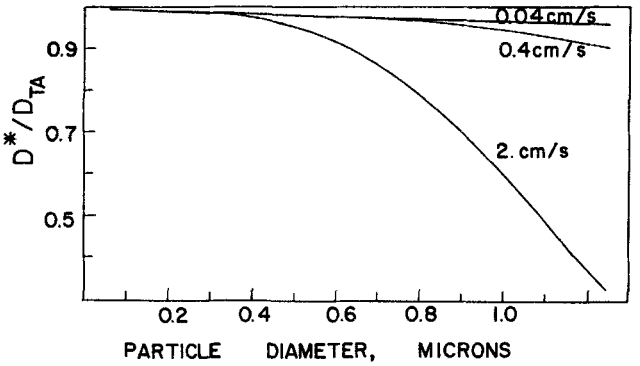

Figure 4. Theoretical results for the dimensionless axial diffusion coefficient of colloidal particles vs. particle size at different eluant average velocities.

Colloidal forces not included; capillary diameter, 60 μm.

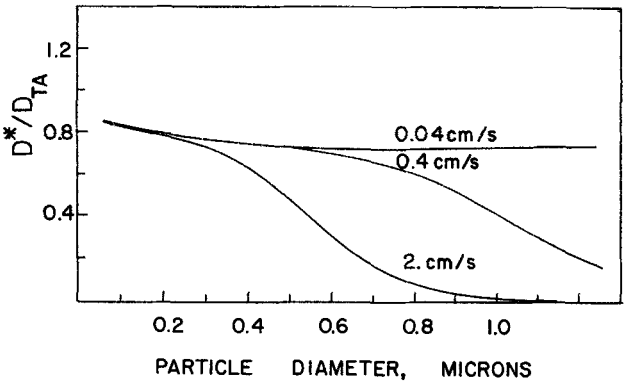

Figure 5. Theoretical results for the dimensionless axial diffusion coefficient of colloidal particles vs. particle size at different eluant average velocities.

Electrolyte concentration, 1 mM; capillary diameter, 6 μm.

the product of the particle Reynolds and Peclet numbers is proportional to the fourth power of the particle radius. For particles larger than 0.1 μm in radius, the inertial forces become significant, and these larger particles will be subject to a greater radial lift force which will reduce the effective axial dispersion coefficient by forcing the particles to migrate away from the region near the wall of the tube.

In general, for the same particle size and eluant velocity, an increase in the radius of the capillary will increase both the dimensionless effective diffusion coefficient and the Taylor-Aris diffusion coefficient.

Since the effect that the inertial force has on the flow behavior of the particles depends mainly on the value of the product Re_pPe, it is expected that a criterion can be established, based on this product, in order to determine the onset of inertial forces, as well as the conditions under which the inertial forces become the controlling mechanism of axial dispersion. We found that variations in the dimensionless effective axial diffusion coefficient, compared to those values obtained at zero particle radial velocity, begin to occur when $Re_pPe = 0.1$. For values of $Re_pPe > 0.1$, we found that as the product of Re_pPe increases (by either increasing the particle size and/or the fluid velocity, or by decreasing the capillary diameter), the dimensionless effective diffusion coefficient decreased monotonically.

Effect of colloidal forces

The role of the colloidal forces on the mean axial diffusion coefficient is illustrated in Figures 5 to 8. Following Fowkes (1964), the value for the Hamaker constant for polystyrene in water, 5×10^{-14} erg, was used. Values reported for the zeta potential of polymer latexes are generally within the range of 20 to 150 mV and usually display an ionic strength dependence, indicative of the constancy of the surface charge density. In these calculations, values of 1.5×10^4 statCoulomb/cm^2 and 30 mV were used for the surface charge density of the particles and the surface potential of the capillary wall. The surface potential of the particles was evaluated by substituting the surface charge density into Eq. 26. The characteristic wavelength of the dispersion interaction for polystyrene used was 1.46×10^{-5} cm (Ottewill and Shaw, 1966). These are the same parameters used by Silebi and McHugh (1978) in the analysis of hydrodynamic chromatography. Figures 5 and 6 show the dimensionless mean axial diffusion coefficient for the same geometry and flow conditions as in Figures 2 and 3, but in this case we included the colloidal forces, with a 1-mM electrolyte concentration. One important difference between these results and those in Figures 3 and 4 is that at this electrolyte concentration where double-layer repulsive forces are significant, the dimensionless effective dispersion coefficient is decreased. This effect is more noticeable for smaller particles for which the inertial forces are not significantly large. In the case of larger particles, the influence of the colloidal forces is detected only at very small velocities where $Re_pPe < 30$. For values of this product greater than 30, the colloidal forces are very small compared to the inertial forces; under these conditions, their effect on the effective diffusion coefficient is negligible.

Figures 7 and 8 show the effect of changing the ionic strength of the eluant on the dimensionless mean axial diffusion coefficient for both a small- (6 μm), and a large-diameter (60 μm) capillaries. As can be seen in these two figures, the dimensionless effective axial diffusion coefficient decreases in general, as the ionic strength of the eluant decreases. It is well known that the electrostatic double-layer repulsive force between two surfaces (colloidal particle and capillary wall) increases, when the

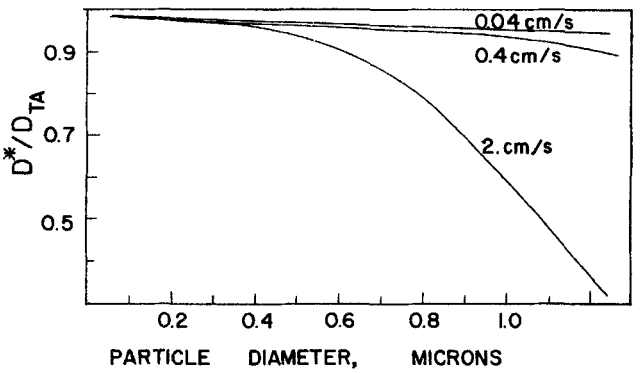

Figure 6. Theoretical results for the dimensionless axial diffusion coefficient of colloidal particles vs. particle size at different eluant average velocities.

Electrolyte concentration, 1 mM; capillary diameter, 60 μm.

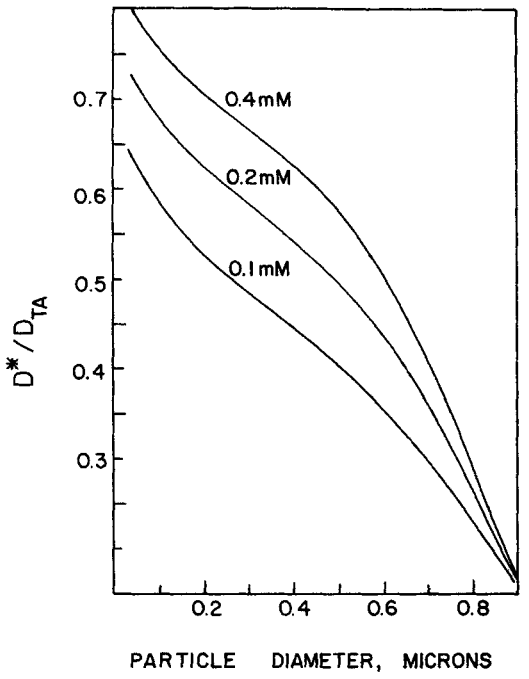

Figure 7. Theoretical results for the dimensionless axial diffusion coefficient of colloidal particles vs. particle size at different eluant ionic strengths.
Eluant velocity, 1 cm/s; capillary diameter, 6 μm.

ionic strength of the medium decreases. Thus, as the ionic strength of the eluant decreases, the particles will be pushed farther away from the capillary wall, therefore sampling faster streamlines which causes a decrease in the effective axial diffusion coefficient.

An interesting feature observed in the case of smaller-diameter capillary (Figure 7) is the convergence of the curves as the particle diameter increases. This convergence is due to the magnitude of the inertial forces, which increase with increasing particle size relative to the colloidal forces. Under these flow conditions, $PeRe_p = 26$ for a 1-μm-diameter particle; therefore, the

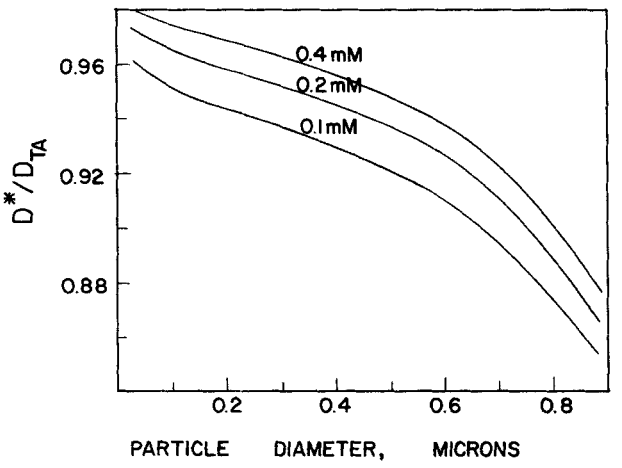

Figure 8. Theoretical results for the dimensionless axial diffusion coefficient of colloidal particles vs. particle size at different eluant ionic strengths.
Eluant velocity, 1 cm/s; capillary diameter, 60 μm.

inertial force acting on this particle is significantly greater than the colloidal forces (which are of shorter range and decay exponentially in the radial direction away from the surface of the capillary). On the other hand, in the case of the larger-diameter capillary, where $PeRe_p < 2.6$, a set of essentially parallel curves for each ionic strength is obtained for particles of 1 μm and less in diameter.

It is also important to emphasize that, for the larger capillary diameter, the decrease as well as the relative change in the effective axial diffusion coefficient with ionic strength for each particle size is very small compared to those variations obtained with the smaller diameter capillary. This indicates that for capillary tubes of 60 μm or more in inner diameter, the eluant ionic strength does not affect significantly the mean axial diffusion coefficient of colloidal particles in CHDF.

Background and Experimental Details

The experimental details of our instrument have been described elsewhere (Silebi and DosRamos, 1988), a diagram of the instrument is shown in Figure 9. It can be briefly described that, from a reservoir, a solution of surfactant is pumped by a Laboratory Data Control minipump (model 2396-57) equipped with a pulse dampener. The surfactant solution flows through the injection valve (Rheodyne 7413) where the sample (5 μL) is loaded and injected into the continuously flowing surfactant solution. This eluant is split into two streams at the exit of the injection valve. The largest portion is sent to a split-flow capillary, while the other portion flows into the capillary column (Polymicro Technologies) where size fractionation of the colloidal particle takes place.

The eluant exiting the capillary is mixed with fresh surfactant (which acts as scavenger or "make-up" fluid) delivered by a consta/metric 3000 constant flow rate duplex minipump (Laboratory Data Control) equipped with a pulse dampener. A SM4000-programmable UV light detector fitted with a 14-μL flow cell (Laboratory Data Control) is utilized to continuously monitor the tubidity of the resulting mixture as a means of determining the residence time of colloidal species in the capillary column. The capillary column consists of an open-fused silica capillary tube, which is 1 to 20 m long and 4 to 68 μm in inner diameter, formed into a 10-cm-diameter coil. Sample splitting at the injection valve and addition of "make-up" fluid at the detector are used to achieve the small sample volumes and low flow rates required due to the small capillary inner volume. The detector has been interfaced to a Zenith Z-148 microcomputer equipped with a math coprocessor which reads the eluant turbidity every 0.5 s and stores these values on the microcomputer hard disk for data analysis.

Since the flow in the capillary is laminar, with tube Reynolds numbers ranging from 0.01 to 12, the internal diameter of the

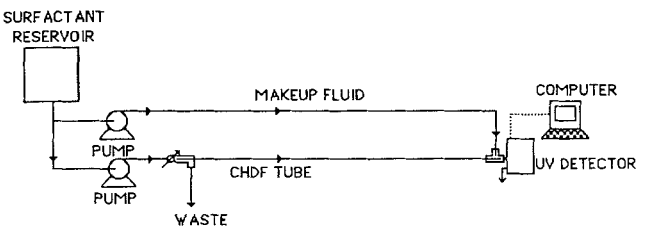

Figure 9. Experimental setup.

capillaries used for the theoretical predictions were determined hydrodynamically by substituting the tube length, pressure drop, marker residence time, and fluid viscosity into the well-known Hagen-Poiseuille equation (Bird et al., 1960):

$$R_o = \sqrt{\frac{8\mu L\langle v_m\rangle}{(-\Delta P)}} \tag{38}$$

where the average velocity of the marker is given by the ratio of tube length to mean residence time. Values of R_o from the manufacturer were found to agree well with those calculated from the Hagen-Poiseuille equation.

Dispersion data for flow through capillaries 4–34 μm in diameter at various eluant average velocities were obtained by using well-characterized polystyrene latex particles (0.088–1.1 μm in diameter) dispersed in aqueous solutions containing sodium lauryl sulfate in the concentration range of 0.1 to 40 mM. Dispersion measurements were also made with a molecular size solute, $Na_2Cr_2O_7$, in order to evaluate the contributions of dead volume outside the capillary tube due to the injection and detection cells.

Since a fractogram is fundamentally a time distribution of the concentration of sample in the eluting stream, the axial dispersion in capillary tubes can be determined experimentally from the fractogram generated by the detection of the injected sample as it exits from the capillary tube. The spreading of the fractogram is characterized by the axial dispersion coefficient which can be evaluated from the variance, σ_t^2, of the fractogram given by:

$$\sigma_t^2 = \frac{\int_0^\infty (t - \langle t_s\rangle)^2 S(t)\, dt}{\int_0^\infty S(t)\, dt} \tag{39}$$

where $\langle t_s\rangle$ is the average elution time of the sample, and $S(t)$ is the detector response, which in the case of a photometer is related to as the optical density. The optical density is related to the mean particle concentration, C_m (given by Eq. 37), and the particle scattering cross section, R_{sc}, by:

$$S(t) = C_m R_{sc} K \tag{40}$$

where K is the detector cell pathlength. In order to express this variance in units of particle displacement, σ_l^2, the time variance is multiplied by the square of the sample average axial velocity, $\langle v_s\rangle$; thus,

$$\sigma_z^2 = \sigma_t^2 \langle v_{p_z}\rangle^2 \tag{41}$$

The term plate height, H_{TP}, used frequently as a dispersion parameter, can be defined as the distance-based variance in the peak width per unit length of axial displacement, Z; thus, the plate height is given by:

$$H_{TP} = \frac{\sigma_z^2}{Z} \tag{42}$$

The total mixing associated with the separation of submicron particles by CHDF is composed of the contributions from the mixing at the injection valve, the capillary tube, and the detector. This can be quantified in terms of the variance or second moment of the fractogram as follows:

$$\sigma_z^2 = \sigma_c^2 + \sigma_{n-i}^2 \tag{43}$$

or in terms of the plate height:

$$H_{TP} = H_c + H_{n-i} \tag{44}$$

where σ_T^2 is the total fractogram variance calculated from the detector output, σ_c^2 is the contribution to the total variance from the flow trough the capillary (obtained from the theoretical analysis), and σ_{n-i}^2 represents the additional variance due to the nonidealities in the system. Similarly, H_{TP}, H_c, and H_{n-i} represent the height of a theoretical plate obtained from the fractogram, and the contributions due to axial dispersion through the capillary and the nonidealities (dead volume effects). The contribution from the non-idealities was calculated from the difference between the ideal degree of axial dispersion of a solute (sodium dichromate) flowing through the capillary according to the theory developed by Taylor (1954), and the total experimental dispersion of this solute on our CHDF system. The effect of the nonidealities is illustrated in Figure 10. The theoretical plate height obtained from the fractogram (upper set of points) and the theoretical plate height due to axial dispersion in the capillary (lower set of points) differ by a constant value. This difference corresponds to the contributions from the nonidealities to the second moment of the fractogram obtained at the same flow conditions. As described before, these nonidealities are calculated from the difference between Taylor's analysis for molecular species in solution flowing through a tube under laminar flow conditions and, the axial dispersion coefficient determined experimentally with sodium dichromate.

Comparison of Theory and Experiment

Figures 10 to 15 show a comparison between the experimental results and those calculated by the theoretical analysis. The numerical results obtained using the theoretical analysis de-

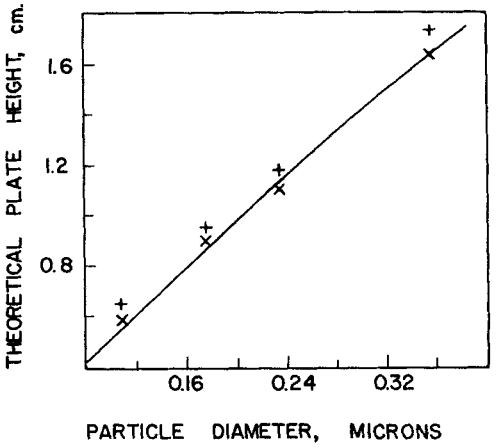

Figure 10. Comparison of theoretical and experimental results for the theoretical plate height of colloidal particles vs. particle size.

+, total instrumental dispersion; X, dispersion due to the capillary; curve, theoretical calculation; capillary diameter, 12 μm; surfactant, 10^{-3} M SLS; v_m, 2.3 cm/s.

scribed above were compared to results obtained experimentally using our CHDF system. The axial dispersion of submicron particles was quantified in terms of the height of a theoretical plate, H_c, due to the axial dispersion in the capillary. The experimentally-determined height of a theoretical plate and the theoretically-calculated values are shown in Figures 10–15 for different particle sizes, eluant average velocities, capillary diameters, and eluant ionic strengths. The fitting between the experimental and the theoretical results is excellent.

Figure 11 presents the effect of particle size on H_c at three different eluant average velocities. It can be observed that at low velocities H_c increases with increasing particle size and increasing eluant average velocity. The convective contribution to axial dispersion (given by the first term in Eq. 36) is the controlling mechanism in liquids and increases with decreasing the diffusion coefficient of the solute species (larger particle size). Consequently, it is expected that H_c would show this behavior. As shown below, this holds for the cases in which the lift force is relatively small, corresponding to values of $Re_pPe < 10.5$. This is the case for the eluant average velocities and particle sizes studied in this figure except for the larger particle at the highest eluant velocity for which this product is equal to 10.5. It can be observed that in this system the height of a theoretical plate for the larger particle is not linear and that it reaches a maximum at a velocity corresponding to $Re_pPe = 10.5$. Also it should be noted that under this conditions, in which the inertial forces become important, the height of a theoretical for the smaller particle (0.176 μm) is the same as that for the larger particle (0.357 μm).

Figures 12 and 13 show the effect of the eluant average velocity and particle size on the height of a theoretical plate in a 34-μm-diameter tube. In Figure 12 $Re_pPe < 4$, while in Figure 13 $Re_pPe > 4$. Figure 12 shows the value of H_c for 0.357- and 0.088-μm particles using a 34-μm-diameter capillary. It can be seen that the theoretical plate height increases as the eluant average velocity increases. It can also be observed that the 0.088-μm particles produce a straight line for this figure which resembles the linear relationship predicted for H_c from Taylor's analytical expression; however, smaller H_c values are obtained due to the size exclusion effect and the colloidal and inertial

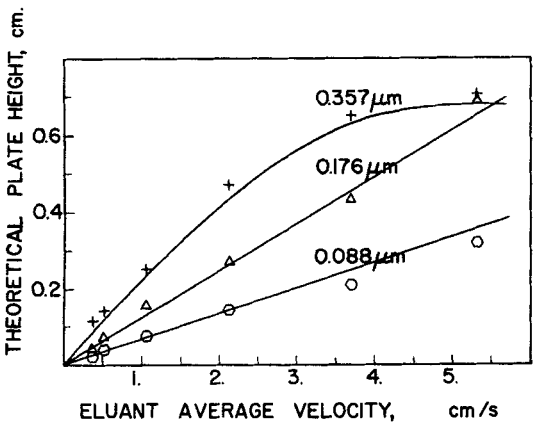

Figure 11. Comparison between theoretical and experimental results for the theoretical plate height of colloidal particles vs eluant average velocity.

Capillary diameter, 6.4 μm; surfactant, 10^{-3} M SLS.

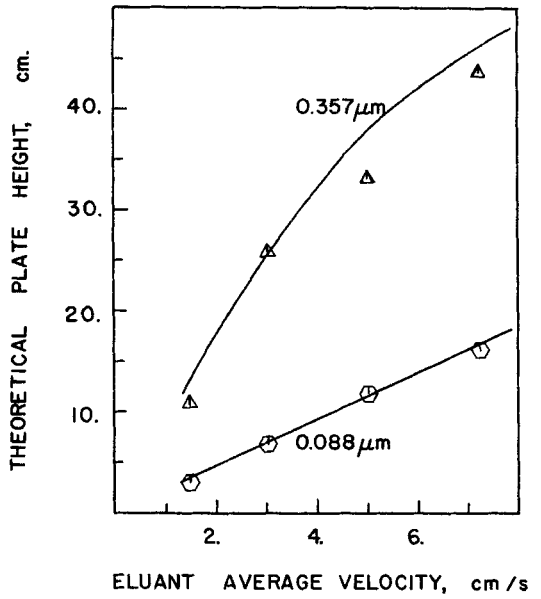

Figure 12. Comparison between theoretical and experimental results for the theoretical plate height of colloidal particles vs. eluant average velocity.

Capillary diameter, 34 μm; surfactant, 10^{-3} M SLS.

forces. On the other hand, the 0.357-μm particles do not display this linear dependence. As the eluant velocity increases, the curve slope decreases, eventually approaching a maximum theoretically at a velocity of 11.5 cm/s. These results indicate that, as the particles become smaller, their behavior approaches that of a solute. A maximum (such as the one displayed by the larger particles in Figure 13), however, should be obtained for the

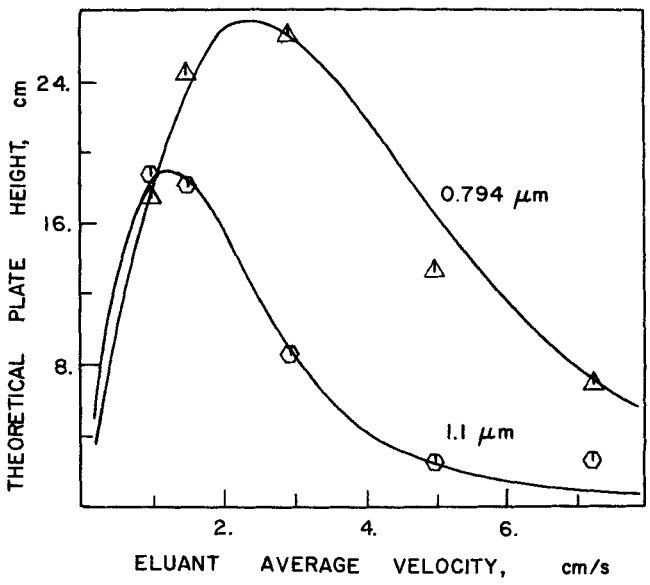

Figure 13. Comparison between theoretical and experimental results for the theoretical plate height of colloidal particles vs. eluant average velocity.

Capillary diameter, 34 μm; surfactant, 10^{-3} M SLS.

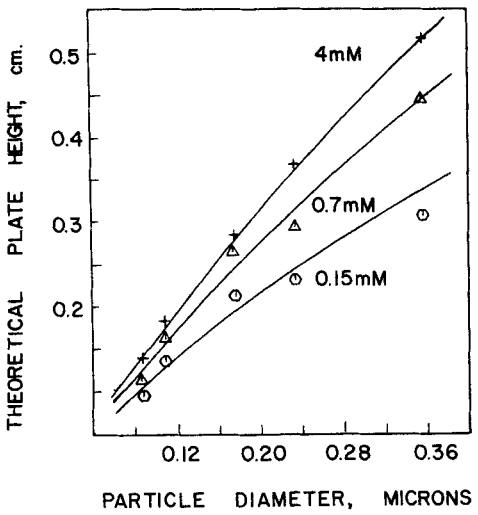

Figure 14. Comparison between theoretical and experimental results for the theoretical plate height of colloidal particles vs. particle size.
Capillary diameter, 7 μm; eluant average velocity, 1.3 cm/s.

smaller particles, if the eluant average velocity is increased to higher values where the inertial forces become significant.

Figure 13 shows the calculated theoretical plate height, H_c, in the case of a 34-μm-ID capillary tube for 1.1 and 0.794 μm particles. As observed, a maximum in the value of the height of a theoretical plate is obtained as a function of the eluant average velocity for every particle size. Calculations using the theoretical analysis described before predict that this maximum occurs at values of $Re_pPe = 10.5$. Thus, for larger particles, which reach this value at smaller fluid velocities, the theoretical plate height is maximum at smaller values of the eluant average velocity. Moreover, as can be seen from both the theoretical and

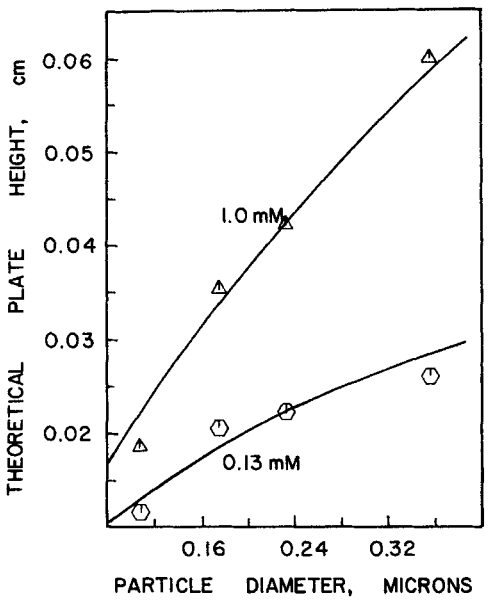

Figure 15. Comparison between theoretical and experimental results for the theoretical plate height of colloidal particles vs particle size.
Capillary diameter, 4.1 μm; eluant average velocity, 0.75 cm/s.

experimental results, the theoretical plate height is smaller for the larger particles at velocities for which this product is greater than 10.5. Conversely, at eluant average velocities below the maximum, the theoretical plate height is larger for larger particles. As indicated before, this occurs because the lift force is not sufficiently strong at these values of eluant average velocity; therefore, the main mechanism governing the particle radial displacement at these low eluant average velocities are the particle radial diffusion and the colloidal forces, resulting in lower axial dispersion for species having larger diffusivity (smaller particle size).

The effect of the eluant ionic strength is illustrated in Figures 14 and 15 for capillaries with diameters of 7 and 4.1 μm, respectively. These figures show that, as theoretically predicted, the effective axial dispersion coefficient and consequently the height of a theoretical plate H decreases as the eluant ionic strength decreases, because the electric double-layer repulsive force between the colloidal particles and the capillary wall increases and particles are forced to sample streamlines farther away from the capillary wall. It is also observed in these two figures that the relative effect of the electrostatic repulsion is more pronounced with the smaller capillary diameter in agreement with the theoretical calculations.

Conclusions

The effects of capillary diameter, eluant ionic strength, and eluant average velocity on the axial dispersion of colloidal particles flowing through a capillary tube under laminar flow were studied both theoretically and experimentally. The theoretical analysis developed is based on the evaluation of the different forces acting on the colloidal particles traveling in Poiseuille flow through a capillary conduit. This mathematical model is capable of predicting both the average velocity of the particles as well as the degree of axial dispersion of colloidal particles, i.e., the degree of efficiency of separation of different sizes using the relevant experimental conditions. The results are predicted from first principles without use of any adjustable parameters. Excellent agreement between the predicted and experimental results is found; this is specially significant because of the absence of adjustable parameters in the analysis.

It is observed that the axial dispersion of colloidal particles is a function of the ratio of particle to capillary radii, and the eluant ionic strength and average velocity. At low eluant average velocities, since the product Re_pPe is less than 10.5, the degree of axial dispersion is larger for the larger particles. On the other hand, at large eluant average velocities and with $Re_pPe > 10.5$, the behavior is the opposite. This is due to the influence of the lift force on the particles. The lift force decreases the degree of axial dispersion and is larger for larger particles and larger eluant average velocities. This effect is better quantified by the product of the particle Reynolds and Peclet numbers. At values of this product above 30, the inertial force is dominant and the colloidal forces have very little influence in the effective axial diffusivity of the particles. At values of this product below 0.1, the inertial forces are negligible and the effective diffusion coefficient is solely affected by the colloidal forces. The height of a theoretical plate of a colloidal particle, which depends upon the degree of axial dispersion, is maximum when the product Peclet and particle Reynolds number are equal to 10.5, indicating that at this condition the inertial force becomes noticeable, pushing the particles to move away from

the wall of the capillary and consequently decreasing the degree of axial dispersion.

Notation

a = minimum separation distance between particle and capillary wall, cm
A = integration constant for solute concentration, particles/cm^3
A_H = Hamaker constant, erg
c_i = ionic concentration in the eluant, mol/cm^3
C = solute concentration, particles/cm^3
C_m = mean solute concentration, particles/cm^3
D^* = effective axial diffusivity, cm^2/s
D_i = i component of the diffusion coefficient tensor, cm^2/s
D_∞ = particle diffusion coefficient, cm^2/s
D_p = particle diameter, cm
e = protonic charge, C
F_H = hydrodynamic resistance to particle displacement, dyne
$f_i(h/R_o)$ = correction to Stokes' law for a particle moving near a wall in the i direction
$f_1(r/R_o), f_2(h/R_o)$ = radial migration velocity functions for neutrally buoyant particles
$g(r/R_o)$ = radial migration velocity function for nonneutrally buoyant particles
H_{TP} = theoretical plate height, cm
H_c = capillary contribution to the height of a theoretical plate, cm
H_{ni} = contribution of the nonidealities to the height of a theoretical plate, cm
$h(r/R_o)$ = radial migration velocity function for particles in a quiescent fluid
k = Boltzmann Constant, 1.38×10^{-16} erg/K
L = capillary length, cm
N = total particle flux tensor, particles · cm^{-2} · s^{-1}
N_z = longitudinal particle flux, particles · cm^{-2} · s^{-1}
N_{z_1} = rate of transport of particles across a plane of constant Z_1, particles · cm^{-2} · s^{-1}
ΔP = capillary pressure drop, Pa
Pe = Peclet number, $R_o v_m / D_\infty$
r = radial distance from axis, cm
Re = tube Reynolds number, $2R_o v_m/\nu$
Re_p = particle Reynolds number, $2R_p v_{s_p}(0)/\nu$
R_f = separation factor equal to the ratio of particle to eluant average velocities in the capillary
R_o = capillary inner radius, cm
R_p = particle radius, cm
$\langle v_{p_z} \rangle$ = particle mean axial velocity, cm/s
v_m = eluant average velocity, cm · s^{-1}
v_{p_r} = particle radial velocity, cm/s
v_{p_s} = particle axial slip velocity, cm/s
v_{p_z} = particle local longitudinal velocity, cm/s
z = electrolyte valence
Z = distance from tube entrance, cm
Z_1 = axial distance with respect to a coordinate system moving with velocity v_m, cm

Greek letters

ϵ = eluant dielectric constant
Φ = total interaction potential, erg
Φ_{DL} = electrostatic double-layer potential, erg
Φ_{vw} = van der Waals potential of interaction, erg
κ = ratio of particle radius to tube radii radius
κ_D = debye double-layer thickness, cm
λ = wavelength of intrinsic oscillations of atoms, cm
μ = eluant viscosity, g/cm · s
ν = eluant kinematic viscosity, cm^2/s
σ_z^2 = variance of the longitudinal displacement, cm^2
σ_t^2 = variance of the residence time distribution, s^2
σ_T^2 = total longitudinal variance of the fractogram, cm^2
σ_q = surface charge density, C/cm^2
ψ_i = capillary ($i = 1$), or particle ($i = 2$) surface potentials, erg

Literature Cited

Ananthakrishnan, V., W. N. Gill, and A. J. Barduhn, "Laminar Dispersion in Capillaries: I. Mathematical Analysis," *AIChE J.*, **11**, 1063 (1965).

Aris, R., "On the Dispersion of a Solute in a Fluid Flowing in a Tube," *Proc. Roy. Soc.*, **A235**, 67 (1956).

Bailey, H. R., and W. B. Gogarty, "Numerical and Experimental Results on Dispersion of a Solute in a Fluid in Laminar Flow through a Tube," *Proc. Roy. Soc., London*, **252A**, 538 (1959).

Bell, G. M., S. Levine, and L. N. McCartney, "Approximate Methods of Determining the Double-Layer Free Energy of Interaction between Two Charged Colloidal Spheres," *J. Colloid Interf. Sci.*, **33**, 335 (1970).

Bird, R. B., W. E. Stewart, and E. N. Lightfoot, *Transport Phenomena*, Wiley, New York (1960).

Brenner, H., "Hydrodynamic Resistance of Particles at Small Reynolds Numbers," *Adv. in Chem. Eng.*, **6**, 287 (1966).

Brenner, H., and L. J. Gaydos, "The Constrained Brownian Movement of Spherical Particles in Cylindrical Pores of Comparable Radius: Models of the Diffusive and Convective Transport of Solute Molecules in Membranes and Porous Media," *J. Colloid Interf. Sci.*, **58**, 312 (1977).

Brenner, H., and J. Happel, "Slow Viscous Flow Past a Sphere in a Cylindrical Tube," *J. Fluid Mech.*, **4**, 195 (1958).

Brough, A. W. J., D. E. Hillman, and R. W. Perry, "Capillary Hydrodynamic Chromatography: an Investigation into Operational Characteristics," *J. Chromat.*, **208**, 175 (1981).

Buffham, B. A., "Model Independent Aspects of Hydrodynamic Chromatography Theory," *J. Colloid Interf. Sci.*, **67**, 154 (1978).

Bungay, P. M., and H. Brenner, "Pressure Drop due to the Motion of a Sphere Near the Wall Bounding a Poiseuille Flow," *J. Fluid Mech.*, **60**, 81 (1973).

Cox, R. G., and H. Brenner, "The Lateral Migration of Solid Particles in Poiseuille Flow: I. Theory," *Chem. Eng. Sci.*, **23**, 147 (1968).

Cox, R. G., and S. K. Hsu, "The Lateral Migration of Solid Particles in a Laminar Flow near a Plane," *Int. J. Multiphase Flow*, **3**, 201 (1977).

DiMarzio, E. A., and C. M. Guttman, "Separation by Flow," *Macromol.*, **3**, 131 (1970).

de Jaeger, N. C., J. L. Trappers, and P. Lardon, "An Investigation into Capillary Hydrodynamic Chromatography," *Part. Charact.*, **3**, 187 (1986).

DosRamos, J. G., "Separation of Submicron Particles by Flow Fractionation: Capillary Hydrodynamic Fractionation (CHDF)," PhD Thesis, Lehigh Univ. (1988).

Evans, E. V., and C. N. Kenney, "Gaseous Dispersion in Laminar Flow through a Circular Tube," *Proc. Roy. Soc.*, London, **284A**, 540 (1965).

Goldsmith, H. L., and S. G. Mason, "The Flow of Suspensions through Tubes: I. Single Spheres, Rods, and Discs," *J. Colloid Interf. Sci.*, **17**, 448 (1962).

Goldsmith, H. L., and S. G. Mason, "Axial Migration of Particles in Poiseuille Flow," *Nat.*, **190**, 1095 (1961).

Goldsmith, H. L., and S. G. Mason, "The Microrheology of Suspensions," *Rheology: Theory and Applications*, F. R. Eirich, ed., Vol. 4, Academic Press (1966).

Gregory, J., "Approximate Expressions for Retarded van der Waals Interaction," *J. Colloid Interf. Sci.*, **83**, 138 (1981).

Guttman, C. M., and E. A. DiMarzio, "Separation by Flow: II. Application to Gel Permeation Chromatography," *Macromol.*, **3**, 681 (1970).

Halow, J. S., and G. B. Wills, "Radial Migration of Spherical Particles in Couette systems," *AIChE J.*, **16**, 281 (1970).

Hamaker, H. C., "The London-van der Waals Attraction between Spherical Particles," *Physica*, **4**, 1058 (1937).

Happel, J., and H. Brenner, *Low Reynolds Number Hydrodynamics*, Martinus Nijhoff, Netherlands (1983).

Happel, J., and B. J. Byrne, "Motion of a Sphere and Fluid in a Cylindrical Tube," *Industrial and Engineering Chemistry*, **46**, 1181 (1954).

Hasimoto, H., "Slow Motion of a Small Sphere in a Cylindrical Domain," *J. Phys. Soc. Jpn.*, **42**, 1047 (1977).
Hirschfield, B. R., H. Brenner, and A. Falade, "First- and Second-Order Wall Effects upon the Slow Viscous Asymmetric Motion of an Arbitrarily-Shaped, –Positioned and –Oriented Particle within a Circular Cylinder," *PHC*, **5**(2), 99 (1984).
Ho, B. P., and L. G. Leal, "Inertial Migration of Rigid Spheres in Two-Dimensional Unidirectional Flows," *J. Fluid Mech.*, **65**, 365 (1974).
Ishii, K., and H. Hasimoto, "Lateral Migration of a Spherical Particle in Flows in a Cylindrical Tube," *J. Phys. Soc. Jpn.*, **48**, 2144 (1980).
Jeffrey, R. C., and J. R. A. Pearson, "Particle Motion in Laminar Vertical Tube Flow," *J. Fluid Mech.*, **22**, 721 (1965).
Karnis, A., H. L. Goldsmith, and S. G. Mason, "Axial Migration of Particles in Poiseuille Flow," *Nat.*, **200**, 159 (1963).
Karnis, A., H. L. Goldsmith, and S. G. Mason, "Flow of Suspensions through Tubes: V. Inertial Effects," *Can. J. Chem. Eng.*, **44**, 181 (1966).
McHugh, A. J., "Particle Size Measurement Using Chromatography," *CRC Crit. Rev. in Analy. Chemistry*, **15**, 63 (1984).
McHugh, A. J., C. A. Silebi, G. W. Poehlein, and J. W. Vanderhoff, "Hydrodynamic Chromatography of Latex Particles," *Colloid and Interface Science*, M. Kerker, ed., Vol. 4, 549, Academic Press, New York (1976).
Mullins, M. E., and C. Orr, "Particle Sizing by Capillary Hydrodynamic Chromatography," *Int. J. Multiphase Flow*, **5**, 79 (1979).
Noel, R. J., K. M. Gooding, F. E. Regnier, D. M. Ball, C. Orr, and M. E. Mullins, "Capillary Hydrodynamic Chromatography," *J. Chromat.*, **166**, 373 (1978).
Oshima, H., T. W. Healy, and L. R. White, "Accurate Analytic Expressions for the Surface Charge Density/Surface Potential Distribution for a Spherical Colloidal Particle," *J. Colloid Interf. Sci.*, **90**, 11 (1982).
Ottewill, R. H., and J. N. Shaw, "Stability of Monodisperse Polystyrene Latex Dispersions of Various Sizes," *Disc. Farad. Soc.*, **42**, 154 (1966).
Ottewill, R. H., and D. J. Wilkins, "Stability of Arachidic Acid Sols," *Trans. Farad. Soc.*, **58**, 608 (1962).
Ploehn, H. J., "Lateral Migration Mechanisms in Capillary Hydrodynamic Chromatography," *Int. J. Multiphase Flow*, **13**, 773 (1987).
Poehlein, S., "Capillary Hydrodynamic Chromatography," unpublished research report, Lehigh Univ., Bethlehem (1978).
Prieve, D. C., and P. M. Hoysan, "Role of Colloidal Forces in Hydrodynamic Chromatography," *J. Colloid Interf. Sci.*, **64**, 201 (1978).
Rubinow, S. I., and J. B. Keller, "The Transverse Force on a Spinning Sphere Moving in a Viscous Fluid," *J. Fluid Mech.*, **11**, 447 (1961).
Saffman, P. G., "The Lift on a Small Sphere in a Slow Shear Flow," *J. Fluid Mech.*, **22**, 385 (1965).
Segre, G., and A. Silberberg, "Behavior of Macroscopic Rigid Spheres in Poiseuille Flow: II. Experimental Results and Interpretation," *J. Fluid Mech.*, **14**, 136 (1962a).
Segre, G., and A. Silberberg, "Radial Particle Displacements in Poiseuille Flow of Suspensions," *Nat.*, **194**, 1269 (1962b).
Shewmon, P. G., *Diffusion in Solids*, McGraw-Hill, New York, 122 (1963).
Silebi, C. A., and J. G. DosRamos, "Separation of Submicron Particles by Capillary Hydrodynamic Fractionation (CHDF)," *J. Colloid Interf. Sci.*, accepted (1989).
Silebi, C. A., and A. J. McHugh, "An Analysis of Flow Separation in Hydrodynamic Chromatography of Latexes," *AIChE J.*, **24**, 204 (1978).
Silebi, C. A., and J. P. Viola, "A Theoretical and Experimental Investigation of Axial Dispersion in Hydrodynamic Chromatography (HDC)," *Org. Coat. Plast. Chem.*, **42**, 151 (1980).
Small, H. J., "Hydrodynamic Chromatography, a Technique for Size Analysis of Colloidal Particles," *J. Colloid Interf. Sci.*, **48**, 147 (1974).
Tachibana, M., "On the Behavior of a Sphere in the Laminar Tube Flows," *Rheol. Acta*, **12**, 58 (1973).
Taylor, G. I., *Proc. R. Soc. Lond.*, "Dispersion of Soluble Matter in Solvent Flowing Slowly through a Tube," **A219**, 186 (1953).
Taylor, G. I., "Conditions under Which Dispersion of a Solute in a Stream of Solvent Can Be Used to Measure Molecular Diffusion," *Proc. R. Soc. Lond.*, **A225**, 473 (1954).
Tijssen, R., J. Bos, and M. E. van Kreveld, "Hydrodynamic Chromatography of Macromolecules in Open Microcapillary Tubes," *Anal. Chem.*, **58**, 3036 (1986).
Vasseur, P., and R. G. Cox, "The Lateral Migration of a Spherical Particle in Two-Dimensional Shear Flows," *J. Fluid Mech.*, **78**, 385 (1976).
Verwey, E. J., and J. Th. G. Overbeek, *Theory of the Stability of Lyophobic Colloids*, Elsevier, Amsterdam (1948).
Walz, D., and F. Grun, "The Radial Velocity of Spherical Particles in Tubular Pinch Effect Experiments," *J. Colloid Interf. Sci.*, **45**, 467 (1973).
Whitmore, R. L., *Rheology of the Circulation*, Pergamon, Oxford (1968).

Manuscript received Dec. 5, 1988, and revision received May 24, 1989.